PP2A inhibitor PME-1 drives kinase inhibitor resistance in glioma cells

Amanpreet Kaur[1,2,3], Oxana V. Denisova[1], Xi Qiao[1,2], Mikael Jumppanen[1], Emilia Peuhu[1], Shafiq U. Ahmed[4,10], Olayinka Raheem[5,6], Hannu Haapasalo[7], John Eriksson[1,8], Anthony J. Chalmers[4], Pirjo Laakkonen[9], and Jukka Westermarck[1,2]

Author affiliations:
[1]Turku Centre for Biotechnology, University of Turku and Åbo Akademi University, Turku, 20520, Finland.
[2]Department of Pathology, University of Turku, Turku, 20520, Finland.
[3]TuBS and TuDMM Doctoral Programmes, Turku, 20520, Finland.
[4]Institute of Cancer Sciences, Wolfson Wohl Cancer Research Centre, University of Glasgow, Glasgow, G61 1QH, UK.
[5]Neuromuscular Research Unit, Tampere University and University Hospital, Tampere, 33520, Finland.
[6]Division of Pathology and Genetics, HUSLAB, Helsinki, 00029, Finland.
[7]Department of Pathology, Fimlab Laboratories, Tampere, 33520, Finland.
[8]Department of Biosciences, Åbo Akademi University, Turku, 20520, Finland.
[9]Research Programs Unit, Translational Cancer Research and Laboratory Animal Centre, University of Helsinki, Helsinki, 00014, Finland.
[10]Department of Pharmacy, Health and Well-being, Dale Building, Sciences Complex, University of Sunderland, SR1 3SD, UK.

Running title: PME-1 drives kinase inhibitor resistance in GBM

Keywords: Cancer, Glioblastoma, Protein phosphatase 2A, Kinase inhibitor resistance

Financial support: J. Westermarck was supported by grants from Sigrid Juselius Foundation, Finnish Cancer Association, Academy of Finland (grant 252572), Jane and Aatos Erkko Foundation, and Medical Research Fund of Tampere University Hospital. A. Kaur was supported by Turku Doctoral Programme of Biomedical Sciences (TuBS), Turku Doctoral Programme of Molecular Medicine (TuDMM), Orion Research Foundation, Cancer Society of Finland, Instrumentarium Science Foundation and K. Albin Johanssons Foundation. A.J. Chalmers received a grant from UK Medical Research Council. J. Westermarck holds a Research Professor position supported by Foundation of the Finnish Cancer Institute.

Address correspondence to: Jukka Westermarck, jukwes@utu.fi

Authors declare no conflicts of interest.

Word count: 5999 (excluding references), Number of figures: 6

Abstract

Glioblastoma multiforme (GBM) lacks effective therapy options. Although deregulated kinase pathways are drivers of malignant progression in GBM, glioma cells exhibit intrinsic resistance towards many kinase inhibitors, and the molecular basis of this resistance remains poorly understood. Here we show that overexpression of the protein phosphatase 2A (PP2A) inhibitor protein PME-1 drives resistance of glioma cells to various multikinase inhibitors. The PME-1-elicited resistance was dependent on specific PP2A complexes and was mediated by a decrease in cytoplasmic HDAC4 activity. Importantly, both PME-1 and HDAC4 associated with human glioma progression, supporting clinical relevance of the identified mechanism. Synthetic lethality induced by both PME-1 and HDAC4 inhibition was dependent on the co-expression of pro-apoptotic protein BAD. Thus, PME-1-mediated PP2A inhibition is a novel mechanistic explanation for multikinase inhibitor resistance in glioma cells. Clinically, these results may inform patient stratification strategies for future clinical trials with selected kinase inhibitors in GBM.

Introduction

Glioblastoma multiforme (GBM) remains extremely difficult to treat (1,2). The failure of targeted therapies in GBM can be linked to inherently high apoptosis-resistance of GBM cells, especially GBM cancer stem cells (GSCs) (3,4). Particularly puzzling is dichotomy between the fact that GBM is driven by receptor tyrosine kinase signaling (1,2), but, specific small molecule kinase inhibitors have failed to provide any clinical benefit in numerous clinical trials (3-5).

The serine/threonine protein phosphatase PP2A dephosphorylates large fraction of cellular serine/threonine phosphorylated proteins, and acts as a major tumor suppressor (6,7). PP2A is a trimeric protein complex in which substrate specificity of the complex is determined by up to 15 different regulatory (B) subunits, which together with the scaffolding (A) and catalytic (C, PP2Ac) subunits generate a large number of alternative PP2A trimers (7,8). PP2A inhibition by overexpression of endogenous inhibitory proteins, or by genetic mutations, results in hyperphosphorylation and activation of various cancer drivers. Consequently, PP2A inhibition contributes to the malignant transformation of human cells, and promotes many malignant phenotypes (6,9).

The endogenous PP2A inhibitor protein, protein phosphatase methylesterase 1 (PME-1) (10), regulates PP2Ac activity by demethylating the highly conserved carboxyl-terminal tail, and by directly binding to the PP2Ac catalytic site (7,11). Notably, PME-1 selectively regulates activity of only certain B-subunit containing PP2A complexes (7). Consequently, as PME-1 does not regulate ubiquitous PP2A activity, only few PP2A phosphoprotein targets have thus far been identified to be affected by PME-1 in cancer

cells. Clinically, PME-1 is expressed in about 50% of human astrocytic gliomas, and its expression levels correlate with the tumor cell proliferation and glioma disease progression (12).

Mammalian HDACs can be classified into four classes (I-IV). The class IIa HDACs (HDAC 4, 5, 7 and 9) shuttle between the nucleus and cytoplasm, and have potential deacetylation targets in both compartments (13). Phosphorylation of HDAC4 facilitates its nuclear export and conversely dephosphorylation by PP2A promotes HDAC4 nuclear import (14,15). More specifically PP2A trimers including PPP2R2A (B55α) and PPP2R5A (B56α) interact with HDAC4 (14,15). Very interestingly, it is the cytoplasmic HDAC4 activity that is important for cell survival particularly in cell types of neuronal origin (16,17).

Here we identify PME-1 as a novel determinant of glioma cell kinase inhibitor resistance. Mechanistically, PME-1 effects are mediated by reactivation of specific PP2A complexes and by consequent decrease in the cytoplasmic HDAC4. The relevance of the findings is validated across several human glioma cell lines and in glioma stem cells, as well as in *in vivo* xenograft model and human glioma tissue samples.

Materials and Methods

Cell culture and transfections

Established human glioblastoma cell lines T98G (VTT Technical Research Centre, Turku, Finland in 2010) and U251MG (from Pirjo Laakkonen, University of Helsinki, Finland in 2011) were cultured in Eagle's MEM (Sigma-Aldrich), and U87MG-luciferase (18) (gift from Ari Hinkkanen, University of Eastern Finland, Finland in 2011) in DMEM (Sigma-Aldrich). All growth mediums were supplemented with 10% heat-inactivated FBS (Gibco), 2 mM L-glutamine and penicillin (50 units/mL)–streptomycin (50 µg/mL) (pen/strep) in a humidified atmosphere of 5% CO_2 at 37°C. T98G and U87MG-luciferase cells lines were authenticated by 16 loci STR profiling (LGC Standards, Middlesex, UK) in 2013. Normal rat astrocytes isolated from the hippocampus region of new born (P0–P1) rat pup brains were kindly provided by Dr. Eleanor Coffey (Turku Centre for Biotechnology, Finland). Astrocytes were cultured on BD matrigel-coated dishes in DMEM supplemented with 10% FBS, L-glutamine and pen/strep.

E2, G7, R10, R15 and R24 primary glioblastoma cell lines were derived from freshly resected GBM specimens as previously described (19) and generously provided by Dr. Colin Watts (University of Cambridge, UK). Tissue collection protocols were compliant with the UK Human Tissue Act 2004 (HTA License 12315) and approved by the local regional Ethics Committee (LREC 04/Q0108/60). Informed consent was obtained from each patient before surgery. Their culture conditions have been described (19) and are included in supplementary materials and methods.

siRNA transfections were performed with Lipofectamine RNAiMAX (Invitrogen, Life technologies). siRNA sequences are in the supplementary table S1. HDAC4-GFP plasmid (20) (gift from Prof. Stuart L. Schreiber, Howard Hughes Medical Institute, USA) was transfected using Fugene HD (Roche) one day after the siRNA transfection.

Chemical inhibitors and drugs

Following chemicals were purchased from indicated distributors: H7, H8, H89, Chelerythrine chloride (Chl Cl), Sunitinib, Tandutinib, Lapatinib and Vandetanib from Biaffin GmbH & Co KG; UO126, LY294002, RO-31-8220, GÖ 6976 and SB218078 from Calbiochem; Staurosporine (STS), CEP-701, UCN-01, PKC412, Z-VAD-FMK, Okadaic acid, Sodium selenite, Xylulose-5-phosphate (X5P), and SB431542 from Sigma-Aldrich; Temozolomide (TMZ), Arcyriaflavin-A and K252c from Tocris Bioscience; K252a and Rebeccamycin from Enzo Life Sciences; Enzastaurin (LC laboratories). FTY720 (Cayman chemicals); Panobinostat and FK228 (MedChem Express); SAHA and ABT263 (Selleckchem). DHPCC-9 (21) was a kind gift from Dr. Päivi Koskinen (University of Turku, Finland). ABL127 (22) kindly provided by Prof. Benjamin Cravatt (The Scripps Research Institute, California, USA).

Apoptosis assay (Nuclear fragmentation assay)

The percentage of the sub-G_0/G_1 fraction of fragmented nuclei stained with propidium iodide (PI) was taken as a measure of apoptotic cells. Approximately 30,000 cells were seeded on 24-well plates, transfected with siRNA for 48 hours, and then treated with test compounds in fresh media. After 24 hours of treatment, both floating and adherent cells were harvested by centrifugation. Cell pellets were resuspended in 400µl of

hypotonic PI buffer, (40mM Tri-sodium citrate (Merck), 0.3% Triton X-100 (Sigma-Aldrich) and 50µg/ml Propidium iodide (Sigma-Aldrich) in PBS), and incubated at room temperature for 10 minutes in dark. The flow cytometric analysis was performed using FACSCalibur (Becton Dickinson) and the recorded data was analyzed with CellQuest Pro software.

ABT263 treatment was performed in combination with STS for 24 hours, starting from one day after seeding cells on 24 well plates. Treatments with PP2A activators FTY720, Sodium Selenate and Xylulose-5-phosphate were performed throughout the experiment starting from one day after seeding cells. Pre-treatment with PP2A inhibitor Okadaic acid were performed for 24 hours before STS treatment. PME-1 inhibitor ABL127 treatment was performed for 24 hours prior to STS treatment. Z-VAD-FMK treatment was performed one day after siRNA transfection for 24 hours followed by combined treatment with STS and fresh Z-VAD-FMK inhibitor treatment for another 24 hours before analysis. HDAC inhibitor treatments were performed for 24 hours alone, followed by combined HDAC and STS or UCN-01 treatment for another 24 hours before staining and FACS analysis.

Colony formation assay

Optimized numbers of cells (2-8 x 10^3) were seeded in 12-well plates until formation of colonies. siRNA transfections were performed using Lipofectamine RNAiMAX reagent (Invitrogen) and after 48 hours, colonies were treated with indicated concentration of chemical drugs for another 48 hours. Cell colonies were fixed with 3.7% formaldehyde and stained with 0.2% crystal violet solution (made in 10% ethanol) for 15 minutes at

room temperature each. Excess stain was removed by repeated washing with PBS. Plates were dried and scanned with Epson perfection V700 scanner. Quantifications were performed with ColonyArea (23) ImageJ (24) plugin and graphs were plotted using the Area % values.

Statistical Analysis

The significance level of differences between the mean values of two groups of data was evaluated using the unpaired Student's t-test assuming unequal variances among the sample means. All p-values were two-tailed. Parameter differences with probability value $p<0.05$ were depicted as statistically significant (*) and $p<0.001$ as highly significant (**).

Correlation between sensitivity of PME-1 or HDAC4 depleted T98G cells towards STS derivatives was analyzed by Pearson's correlation method, where relationships are determined by the correlation coefficient. R +0.4 to +0.69 indicates for strong positive correlation.

Results

PME-1 depletion induces glioma cell synthetic lethality in conjunction with kinase inhibitors

Given the PP2A´s capacity to negatively regulate phosphoproteins, we explored whether reactivation of PP2A activity in PME-1 depleted cells would further predispose glioma cells to apoptosis induction by kinase inhibitors. We employed a series of kinase inhibitors targeting different classes of kinases, mainly grouped under AGC/CAMK (Protein Kinase A, G, C and Calcium/Calmodulin regulated kinases) and TK (Tyrosine kinase) inhibitor categories, and one broad-spectrum kinase inhibitor, Staurosporine (STS). All tested inhibitors showed efficient downregulation of known phosphorylated target proteins (Supplementary Fig. S1A). Consistent with the inherent kinase inhibitor resistance of GBM (3-5,25), no apparent induction of apoptosis was observed by treatment with any of the tested inhibitors in the control siRNA transfected cells (Fig. 1A, grey bars). Also, PME-1 depletion alone did not induce strong apoptotic phenotype (Fig. 1A, black bar in control). In contrast, PME-1 silenced GBM cells displayed enhanced sensitivity to several of kinase inhibitors, most notably observed with H7, Sunitinib, and LY294002 (Fig. 1A, black bars). However, the strongest synthetically lethal activity was observed in PME-1 deficient cells treated with multikinase inhibitor Staurosporine (STS) (Fig. 1A). The STS-induced synthetic lethality in PME-1 silenced cells was dose-dependent, and not due to siRNA off-target effects (Supplementary Fig. S1B-F). Furthermore, the combination of PME-1 inhibition and STS resulted in very efficient inhibition of clonogenicity of both T98G and U251MG glioblastoma cells (Fig. 1B and C). Whereas, the synthetic lethality was not observed in normal astrocytes isolated from the

rat hippocampus (Fig. 1D and Supplementary Fig. S1G), or in other types of cancer cell lines than gliomas (Supplementary Fig. S1H).

Given the potency of STS and its selectivity for gliomas, we focused on STS as a model compound to study the role of PME-1 in mediating kinase inhibitor resistance in glioma cells. Consistent with the nuclear fragmentation assay, we found significantly increased caspase-3/7 activity upon combination treatment (Fig. 1E). Furthermore, pan-caspase inhibitor Z-VAD-FMK, or co-depletion of pro-apoptotic BH3 family protein BAD, completely blocked the apoptosis induction (Fig. 1F-G and Supplementary Fig. S1I). However, BAD activation by a small molecule Bcl-2/-xL inhibitor, ABT263, was not sufficient to synergistically induce apoptosis in combination with STS treatment (Fig. 1H). These results indicate that PME-1 inhibits apoptotic response even in glioma cells with activated BAD.

PME-1 drives resistance to clinically relevant indolocarbazole derivatives in GBM cell lines and in patient derived glioma-stem cells (GSCs)

Many indolocarbazole analogs of STS have more specific kinase inhibition profiles than STS, and are well tolerated in patients (26,27) (Supplementary Table S2). Especially CEP-701 (Lestaurtinib), and PKC412 (Midostaurin) have progressed to phase 3 clinical trials in hematological cancers (Supplementary Table S2). Thus, we screened a collection of STS analogs for synthetic lethality in PME-1 depleted glioblastoma cells. Screening identified PKC412, CEP-701, K252a, and UCN-01 as highly potent synthetically lethal compounds in PME-1 depleted T98G cells (Fig. 2A). These results were validated by colony growth assays using T98G, U251MG, and U87MG glioma cell

lines (Fig. 2B, 2C, Supplementary Fig. S2A and S2B). Moreover, identification of several effective STS derivatives enabled us to perform a structure-activity relationship (SAR) analysis to uncover the structural determinants of indolocarbazole compounds relevant for synthetic lethality in PME-1 depleted cells (Supplementary Table S3).

Importantly, PME-1-driven resistance to active indolocarbazoles is not restricted to *in vitro* cell culture, but occurs also in *in vivo* environment. PME-1 silenced U87MG xenograft tumors showed markedly enhanced responses to UCN-01 as compared to the scrambled siRNA transfected tumors (Fig. 2D and E). In parallel cell cultures, PME-1 siRNA was found to silence PME-1 expression for up to 10 days post-transfection (Supplementary Fig. S2C). Preferential anti-tumorigenic activity of PME-1 siRNA and UCN-01 combinatorial therapy was further validated by intra-tumor delivery of PME-1 siRNA within established U87MG-luc xenograft tumors in mice subsequently treated with UCN-01 (Supplementary Fig. S2D and S2E).

Cancer stem cells (glioma stem cells; GSCs) are important determinants of therapy resistance in glioblastoma (1,28). Therefore, we evaluated whether the results of this study would also be relevant to GSCs (19). The stem cell identity of GSC population was demonstrated by expression of several stem cell markers such as CD133, SOX2, Olig2 and CD15 (Supplementary Fig. S2F). Moreover, we have previously shown that these GSCs display characteristic infiltrative growth pattern in intracranial *in vivo* model (29,30). Indeed, a significant inhibition of colony growth was observed in PME-1 depleted GSCs (E2 and R10 cell lines) treated with either STS or UCN-01 (Fig. 2F-G and Supplementary Fig. S2G-H).

These results demonstrate that PME-1 promotes resistance to multiple clinically applicable indolocarbazole kinase inhibitors in several glioma cell lines, and in the therapy resistant GSCs.

Reactivation of specific PP2A complexes is required for PME-1 depletion-mediated synthetic lethality

As expected, we found elevated phosphatase activity in PP2A immunoprecipitates from PME-1 silenced cells, as compared to those from control cells (Fig. 3A). The inhibition of PP2A catalytic activity by semiselective chemical inhibitor Okadaic acid (OA) in turn rescued the cells from STS-induced synthetic lethality in a dose-dependent manner (Fig. 3B). However, the chemical inhibition of PME-1 methylesterase activity by ABL127 (22) failed to show any synthetic lethality with STS in GBM cells (Supplementary Fig. S3A). Based on these results it is likely that, PME-1-mediated direct inhibition of PP2A catalytic activity (11), rather than its methylesterase activity (10), is relevant for resistance to apoptosis by kinase inhibitors.

Although PP2A has been previously considered as a non-specific housekeeping phosphatase, recent evidence suggests that PP2A complexes differentially regulated by endogenous inhibitor mechanisms selectively dephosphorylate specific targets (7,8) (Fig. 3C). Thereby, we wanted to study whether the observed synthetic lethality could be achieved by other means of PP2A reactivation. Notably, neither depletion of another PP2A inhibitor protein CIP2A (31), nor chemical compounds previously used to reactivate PP2A in cancer cells (32), induced significant synthetic lethality (Fig. 3D, E and Supplementary Fig. S3B).

Next, we wanted to uncover the involvement of specific B-subunit containing PP2A trimers in PME-1-regulated kinase inhibitor resistance. To this end, we employed RNAi-mediated co-depletion of PME-1 with PP2A B-subunits from PPP2R2 and PPP2R5 families, as they have previously been implicated in PME-1-mediated processes (7). Interestingly, depletion of only some members of these B-subunit families, namely PPP2R2A, PPP2R5A and PPP2R5B significantly reduced synthetic lethality (Fig. 3F and Supplementary Fig. S3C). Together these results indicate that the observed synthetic lethality is mediated by specific PME-1-regulated PP2A complexes. Notably, based on cBioPortal TCGA database (33,34), GBM patients do not show genetic alterations in any of the PP2A subunits (Fig. 3G). As PP2A seems to be genetically intact in human gliomas, this indicates that PME-1 overexpression could be a disease relevant mechanism of PP2A inhibition in this disease. Furthermore, inhibition of overexpressed PME-1 in gliomas (12) might result in therapeutic reactivation of genetically intact PP2A phosphatase complexes.

HDAC4 mediates PME-1-driven kinase inhibitor resistance

To discover potential downstream targets of PP2A responsible for PME-1 regulated kinase inhibitor resistance, the existing literature was studied to create a list of proteins known to interact with B-subunits PPP2R2A, PPP2R5A and PPP2R5B (Supplementary Table S4) (35). We inhibited some of these proteins with siRNA or with specific chemical inhibitors, and subsequently treated the cells with the model compound STS (Fig. 4A-B). Interestingly, depletion of MYC and HDAC4 selectively phenocopied the PME-1 depletion-induced synthetic lethality (Fig. 4A-B). Given that HDAC4 was downregulated in cells transfected with MYC siRNA, but HDAC4 siRNA did not affect

MYC expression (Fig. 4C), we postulate HDAC4 is the potential PME-1 target and that the synthetic lethality seen in the MYC silenced cells was also due to HDAC4 inhibition.

Similarly to PME-1, also HDAC4 depletion reduced clonogenicity of STS treated glioma cells (Fig. 4D-E). Importantly, HDAC4 and PME-1 depleted cells showed correlative sensitivity profiles to different indolocarbazole analogs, both in nuclear fragmentation (Fig. 4F and Supplementary Fig. S4A) and in clonogenicity assays (Fig. 4G). HDAC4 depletion also significantly sensitized GSC cultures to STS and UCN-01-induced inhibition of colony growth (Fig. 4H-I). These results were confirmed in another patient derived GSC cell line BT3 and its CD133 enriched subpopulation (Supplementary Fig. S4B-D). Additionally, co-depletion of PME-1 and HDAC4 induced apoptosis as efficiently as depletion of either of them alone (Fig. 4J and Supplementary Fig. S4E). Furthermore, similar to PME-1 (Fig. 1G), simultaneous depletion of BAD and HDAC4 rescued the cells from synthetic lethality (Fig. 4K and Supplementary Fig. S4F). Thus, identical synthetic lethality response profile in PME-1 and HDAC4 depleted cells (Fig. 4F, 4K), and absence of any additive or synergistic effects upon depletion of PME-1 and HDAC4 (Fig. 4J), strongly indicates that HDAC4 mediates PME-1-driven kinase inhibitor resistance in GBM.

Importantly, co-depletion of PPP2R2A B-subunit, implicated in PME-1-depletion induced synthetic lethality (Fig. 3F), did not block synthetic lethality in HDAC4 depleted cells (Fig. 4L). This further indicates that PME-1 and PP2A function upstream of HDAC4. Furthermore, proximity ligation assays (PLA) using anti-HDAC4 together with either anti-PP2A Cα-subunit or anti-PPP2R2A antibodies, revealed a physical association between HDAC4 and this specific B-subunit containing PP2A complex (Fig. 4M).

Loss of cytoplasmic HDAC4 predisposes to kinase inhibitor-induced synthetic lethality

In unperturbed cells, majority of HDAC4 is localized to the cytoplasm, and particularly in certain neuronal cells, the loss of cytosolic HDAC4 has been associated with induction of cell death (16,17,36). Supportive of survival role of cytoplasmic HDAC4 also in glioma cells, we observed predominantly cytoplasmic localization of endogenous HDAC4 in the T98G cells (Fig. 5A), as well as in glioma patient tumor tissue (Fig. 5B). Notably, as shown in figure 4M, also the HDAC4-PPP2R2A association was predominantly localized in the cytoplasm. Consistent with pro-survival activity of cytosolic HDAC4 (16,17,36), PME-1 depletion induced translocation of HDAC4-GFP (20) from cytoplasm to the nucleus (Fig. 5C). Moreover, loss of cytosolic HDAC4 activity upon PME-1 depletion was supported by increased acetylation of several cytosolic proteins, whose acetylation was induced also in HDAC4 depleted cells (Fig. 5D).

Based on previous studies, PME-1 depletion could promote HDAC4 nuclear translocation by dephosphorylation of Ser 298 (14). Unfortunately, due to lack of phospho-Ser 298 HDAC4 antibody, we could not confirm this assumption. Furthermore, we did not observe reduction in the phosphorylation of cytosolic 14-3-3 binding residues, Ser 246 or Ser 632 of HDAC4 by PME-1-depletion (Fig. 5E and Supplementary Fig. S5A). However, in line with previous demonstration of nuclear translocation of HDAC4 upon STS-mediated inhibition of HDAC4 phosphorylating kinases (37,38), HDAC4 phosphorylation at these residues was reduced upon 6 hours treatment with STS (Fig. 5E and Supplementary Fig. S5A). Importantly, total HDAC4 expression was downregulated by combination of PME-1 depletion and STS treatment

(Fig. 5E). Therefore, the combined effects of HDAC4 nuclear translocation by PME-1 depletion, and STS-elicited inhibition of Ser 632 and Ser 246 phosphorylation synergistically inhibit cytoplasmic HDAC4 expression and thus trigger synthetic lethality under STS exposure (Fig. 4B-I).

To address whether existing small molecule HDAC inhibitors could be used to induce synthetic lethality together with STS and its derivatives in glioma cells, we compared effects of three inhibitors, out of which both FK228 (Romidepsin), and Panobinostat inhibit HDAC4 activity in the nanomolar range, whereas SAHA does not (39,40) (Fig. 5F). Indeed, inhibition of HDAC activity by FK228 or Panobinostat showed similar synthetic lethality in combination with STS or UCN-01 treatment as with PME-1 or HDAC4 silencing (Fig. 5G, H and Supplementary Fig. S5B). However, no evidence for synthetic lethal activity was observed in cells co-treated with SAHA (Fig. 5I), even though the tested concentrations of all three HDAC inhibitors were found to inhibit deacetylation of Histone H3 (Supplementary Fig. S5C, yellow bars). Notably, cells treated with FK228 and Panobinostat also showed reduced levels of HDAC4 protein (Supplementary Fig. S5C, green bars), correlating again HDAC4 expression status to sensitivity towards STS-elicited synthetic lethal activity.

Therapeutic vulnerability in human glioblastoma based on PME-1/HDAC4/BAD status

Previously, by immunohistochemistry (IHC) analysis it has been shown that 50% of primary GBM tumors express elevated levels of PME-1 protein (12). Similarly, gene expression analysis using TCGA GBM cohort suggests that about 50% of the patient

tumors also transcribe PME-1 (https://genome-cancer.ucsc.edu/). We speculate that PME-1 protein might be stabilized by post-translational mechanisms in this subpopulation of PME-1 mRNA expressing GBM tumors.

To examine clinical relevance of the PME-1-mediated HDAC4 regulation, we studied HDAC4 status by IHC from the same primary astrocytic glioma patient material as above (12). Importantly, we found a significant correlation between HDAC4 expression and cytoplasmic PME-1 staining ($p=0.049$) (Supplementary Fig. S6A), and similar to PME-1, HDAC4 expression was absent or low in nearly half (41%) of the astrocytic gliomas (Fig. 6A-B). A significant correlation ($p=0.000$) between HDAC4 immunopositivity and the grade of astrocytic tumors was also observed (Fig. 6B).

Based on these data, approximately 50% of glioma patients could display indolocarbazole sensitive phenotype based on their low PME-1 or HDAC4 expression. To mimic glioma cells with constitutively low PME-1 expression, we generated clones of T98G cells stably expressing either GFP (Control) or PME-1 targeting shRNA. In line with the requirement for high PME-1 expression for supporting the growth of high-grade gliomas (12), the maximal tolerated inhibition of PME-1 expression was about 50% (Fig. 6C). Importantly, the isogenic cell lines with modestly reduced PME-1 expression (shRNA PME #1 and #2 clones) showed robust sensitivity to K252a and CEP-701 treatment in both the colony growth (Fig. 6D-E), and the cell viability assays (Supplementary Fig. S6B).

Preferential kinase inhibitor sensitivity of PME-1 and HDAC4 low glioma cells is dependent on the BAD expression (Fig. 1G and 4K). Thereby, we further assessed BAD

immunopositivity from the same patient material. The BAD IHC analysis revealed that about 48% of gliomas exhibited moderate to high BAD expression (Fig. 6A, F and G). Thereby, following the patient tumor PME-1^{low}/BAD^{high}, or HDAC4^{low}/BAD^{high} phenotypes, we were able to identify about 17% and 11% glioma patients, respectively, that constitute the potential responder sub-group to the indolocarbazole kinase inhibitor monotherapies (Fig. 6F, G and H). Alternatively, 37% of glioma patients with HDAC4^{high}/BAD^{high} phenotype could potentially benefit from combination therapy with small molecule HDAC4 inhibitors and selected kinase inhibitors (Fig. 6G and H).

Discussion

Glioma cells exhibit intrinsic resistance to most therapies, which is reflected in dismal clinical response rates (4,5,25). In particular, failure to treat GBM patients with various kinase inhibitors that show clinical activity in other cancer types has been confusing; especially in the light of genetic information that GBM particularly is a disease driven by receptor tyrosine kinase signaling (1,2,34). Here we report PME-1-mediated inhibition of PP2A as an unprecedented explanation of GBM cell resistance to at least reasonable spectrum of different kinase inhibitors.

Inhibition of PP2A tumor suppressor activity is required for malignant transformation of various types of normal cells, and promotes malignancy in many types of human cancers (6,9). However, the functional relevance of PP2A as a tumor suppressor in GBM has not been extensively studied. Interestingly, based on TCGA analysis, GBM harbors very few genetic alterations that would directly affect PP2A complexes (Fig. 3G). Thus, our previous (12), and current identification of PME-1 as a clinically relevant human glioma oncoprotein provide thus far the best understood mechanism how PP2A is inhibited in human gliomas and in GBM. PME-1 is known to affect the activity of only certain PP2A complexes (7). Consistently, we found remarkable selectivity among PP2A B-subunit containing complexes that mediate PME-1-driven kinase inhibitor resistance (Fig. 3F and Supplementary Fig. S3C).

HDAC4 associates with PP2A B-subunits identified here to mediate PME-1 depletion-induced synthetic lethality (Fig. 4M) (17,41). On the other hand, loss of cytosolic HDAC4 has been shown to induce apoptosis in neuronal models (16,17,36). We extend these

findings by showing for the first time that in human glioma patient samples HDAC4 is predominantly cytosolic, and that acetylation of yet to be identified cytosolic proteins is regulated by PME-1 in glioma cells. Role for HDAC4 as a critical target for PME-1-driven kinase inhibitor resistance was further validated by significant correlation of PME-1 and HDAC4 function towards a library of STS derivatives (Fig. 4F-G), as well as by induction of synthetic lethality by small molecule inhibitors of HDAC4 activity in combination with UCN-01 and STS. Naturally, based on our data we cannot exclude potential contribution of other PP2A target proteins in mediating at least partly the PME-1-driven kinase inhibitor resistance phenotype. Clearly highlighting the potential clinical applicability of our results for future GBM therapy, Panobinostat and FK228 have been approved for therapy of multiple myeloma and cutaneous T cell lymphoma, respectively (42,43), and with Panobinostat clinical trials have been conducted in adult gliomas and are underway in pediatric gliomas (44,45)

BAD was shown to be essential for synthetic lethality induced by either PME-1 or HDAC4 depletion. BAD acts as a node between upstream survival signaling pathways and downstream apoptosis signaling. However, these results do not rule of the possibility of other BH3-only pro-apoptotic proteins to be involved in this response. Importantly, results with BAD depletion allowed us to further scrutinize potential clinical applicability of our results for diagnostic stratification of GBM patients. Our results indicate that PME-1^{low}/BAD^{high} or HDAC4^{low}/BAD^{high} phenotype in diagnostic GBM biopsy might serve as a biomarker for stratification of patients to treatment with kinase inhibitors such as CEP-701 (Lestaurtinib), and PKC412 (Midostaurin) that are currently being tested in phase 3 clinical trials (www.clinicaltrials.gov). The patients with PME-

1^{high}/BAD^{high} or $HDAC4^{high}$/BAD^{high} tumor phenotype on the other hand, could benefit from the combined PP2A reactivator compound or HDAC4 inhibitor, and kinase inhibitor therapies. The principles of potential future clinical trials based on the proposed scheme are depicted in Fig. 6H.

In summary, results of this study reveal an unprecedented mechanism by which GBM cells can resist cell-killing activity of kinase inhibitors targeting various survival kinase pathways. The work also identifies both PME-1 and HDAC4 as context-dependent survival factors in GBM, and as potential targets for future combination therapies.

Acknowledgements

Authors thank Prof. Ari Hinkkanen, Prof. Benjamin Cravatt, Prof. Stuart L. Schreiber, Dr. Eleanor Coffey, Dr. Päivi Koskinen, Dr. Panu Jaakkola and Dr. Colin Watts for generous support of research materials. Taina-Kalevo Mattila and Inga Pukonen are acknowledged for their skillful assistance and help. Authors are very grateful to Prof. David Virshup and Prof. Johanna Ivaska for critical comments on the manuscript. Turku Centre for Disease Modelling (TCDM) is acknowledged for expert help with mouse experiments.

References

1. Chen J, McKay RM, Parada LF. Malignant glioma: lessons from genomics, mouse models, and stem cells. Cell 2012;149:36-47.

2. Dunn GP, Rinne ML, Wykosky J, Genovese G, Quayle SN, Dunn IF, et al. Emerging insights into the molecular and cellular basis of glioblastoma. Genes Dev 2012;26:756-84.

3. Krakstad C, Chekenya M. Survival signalling and apoptosis resistance in glioblastomas: opportunities for targeted therapeutics. Molecular cancer 2010;9:135.

4. Joshi AD, Loilome W, Siu IM, Tyler B, Gallia GL, Riggins GJ. Evaluation of tyrosine kinase inhibitor combinations for glioblastoma therapy. PLoS ONE 2012;7:e44372.

5. Reardon DA, Wen PY, Mellinghoff IK. Targeted molecular therapies against epidermal growth factor receptor: past experiences and challenges. Neuro Oncol 2014;16 Suppl 8:viii7-13.

6. Westermarck J, Hahn WC. Multiple pathways regulated by the tumor suppressor PP2A in transformation. Trends in molecular medicine 2008;14:152-60.

7. Sents W, Ivanova E, Lambrecht C, Haesen D, Janssens V. The biogenesis of active protein phosphatase 2A holoenzymes: a tightly regulated process creating phosphatase specificity. FEBS J 2013;280:644-61.

8. Virshup DM, Shenolikar S. From promiscuity to precision: protein phosphatases get a makeover. Mol Cell 2009;33:537-45.

9. Perrotti D, Neviani P. Protein phosphatase 2A: a target for anticancer therapy. The lancet oncology 2013;14:e229-38.

10. Ogris E, Du X, Nelson KC, Mak EK, Yu XX, Lane WS, et al. A protein phosphatase methylesterase (PME-1) is one of several novel proteins stably associating with two inactive mutants of protein phosphatase 2A. J Biol Chem 1999;274:14382-91.

11. Xing Y, Li Z, Chen Y, Stock JB, Jeffrey PD, Shi Y. Structural mechanism of demethylation and inactivation of protein phosphatase 2A. Cell 2008;133:154-63.

12. Puustinen P, Junttila MR, Vanhatupa S, Sablina AA, Hector ME, Teittinen K, et al. PME-1 protects extracellular signal-regulated kinase pathway activity from protein phosphatase 2A-mediated inactivation in human malignant glioma. Cancer Res 2009;69:2870-7.

13. Lee P, Murphy B, Miller R, Menon V, Banik NL, Giglio P, et al. Mechanisms and clinical significance of histone deacetylase inhibitors: epigenetic glioblastoma therapy. Anticancer Res 2015;35:615-25.

14. Paroni G, Cernotta N, Dello Russo C, Gallinari P, Pallaoro M, Foti C, et al. PP2A regulates HDAC4 nuclear import. Mol Biol Cell 2008;19:655-67.

15. Cadot B, Brunetti M, Coppari S, Fedeli S, de Rinaldis E, Dello Russo C, et al. Loss of histone deacetylase 4 causes segregation defects during mitosis of p53-deficient human tumor cells. Cancer Res 2009;69:6074-82.

16. Chen B, Cepko CL. HDAC4 regulates neuronal survival in normal and diseased retinas. Science 2009;323:256-9.

17. Li J, Chen J, Ricupero CL, Hart RP, Schwartz MS, Kusnecov A, et al. Nuclear accumulation of HDAC4 in ATM deficiency promotes neurodegeneration in ataxia telangiectasia. Nat Med 2012;18:783-90.

18. Heikkila JE, Vaha-Koskela MJ, Ruotsalainen JJ, Martikainen MW, Stanford MM, McCart JA, et al. Intravenously administered alphavirus vector VA7 eradicates orthotopic human glioma xenografts in nude mice. PLoS ONE 2010;5:e8603.

19. Fael Al-Mayhani TM, Ball SL, Zhao JW, Fawcett J, Ichimura K, Collins PV, et al. An efficient method for derivation and propagation of glioblastoma cell lines that conserves the molecular profile of their original tumours. Journal of neuroscience methods 2009;176:192-9.

20. Grozinger CM, Schreiber SL. Regulation of histone deacetylase 4 and 5 and transcriptional activity by 14-3-3-dependent cellular localization. Proc Natl Acad Sci U S A 2000;97:7835-40.

21. Santio NM, Vahakoski RL, Rainio EM, Sandholm JA, Virtanen SS, Prudhomme M, et al. Pim-selective inhibitor DHPCC-9 reveals Pim kinases as potent stimulators of cancer cell migration and invasion. Mol Cancer 2010;9:279.

22. Bachovchin DA, Mohr JT, Speers AE, Wang C, Berlin JM, Spicer TP, et al. Academic cross-fertilization by public screening yields a remarkable class of protein phosphatase methylesterase-1 inhibitors. Proc Natl Acad Sci U S A 2011;108:6811-6.

23. Guzman C, Bagga M, Kaur A, Westermarck J, Abankwa D. ColonyArea: an ImageJ plugin to automatically quantify colony formation in clonogenic assays. PLoS ONE 2014;9:e92444.

24. Schneider CA, Rasband WS, Eliceiri KW. NIH Image to ImageJ: 25 years of image analysis. Nature methods 2012;9:671-5.

25. Day SE, Waziri A. Clinical trials of small molecule inhibitors in high-grade glioma. Neurosurgery clinics of North America 2012;23:407-16.

26. Gani OA, Engh RA. Protein kinase inhibition of clinically important staurosporine analogues. Natural product reports 2010;27:489-98.

27. Nakano H, Omura S. Chemical biology of natural indolocarbazole products: 30 years since the discovery of staurosporine. The Journal of antibiotics 2009;62:17-26.

28. Singh SK, Hawkins C, Clarke ID, Squire JA, Bayani J, Hide T, et al. Identification of human brain tumour initiating cells. Nature 2004;432:396-401.

29. Mannino M, Gomez-Roman N, Hochegger H, Chalmers AJ. Differential sensitivity of Glioma stem cells to Aurora kinase A inhibitors: implications for stem cell mitosis and centrosome dynamics. Stem Cell Res 2014;13:135-43.

30. Ahmed SU, Carruthers R, Gilmour L, Yildirim S, Watts C, Chalmers AJ. Selective Inhibition of Parallel DNA Damage Response Pathways Optimizes Radiosensitization of Glioblastoma Stem-like Cells. Cancer Res 2015;75:4416-28.

31. Khanna A, Pimanda JE, Westermarck J. Cancerous inhibitor of protein phosphatase 2A, an emerging human oncoprotein and a potential cancer therapy target. Cancer Res 2013;73:6548-53.

32. Lambrecht C, Haesen D, Sents W, Ivanova E, Janssens V. Structure, regulation, and pharmacological modulation of PP2A phosphatases. Methods Mol Biol 2013;1053:283-305.

33. Cerami E, Gao J, Dogrusoz U, Gross BE, Sumer SO, Aksoy BA, et al. The cBio cancer genomics portal: an open platform for exploring multidimensional cancer genomics data. Cancer discovery 2012;2:401-4.

34. Brennan CW, Verhaak RG, McKenna A, Campos B, Noushmehr H, Salama SR, et al. The somatic genomic landscape of glioblastoma. Cell 2013;155:462-77.

35. Eichhorn PJ, Creyghton MP, Bernards R. Protein phosphatase 2A regulatory subunits and cancer. Biochim Biophys Acta 2009;1795:1-15.

36. Mielcarek M, Landles C, Weiss A, Bradaia A, Seredenina T, Inuabasi L, et al. HDAC4 reduction: a novel therapeutic strategy to target cytoplasmic huntingtin and ameliorate neurodegeneration. PLoS Biology 2013;11:e1001717.

37. Liu Y, Randall WR, Schneider MF. Activity-dependent and -independent nuclear fluxes of HDAC4 mediated by different kinases in adult skeletal muscle. J Cell Biol 2005;168:887-97.

38. Di Giorgio E, Brancolini C. Regulation of class IIa HDAC activities: it is not only matter of subcellular localization. Epigenomics 2016.

39. Bradner JE, West N, Grachan ML, Greenberg EF, Haggarty SJ, Warnow T, et al. Chemical Phylogenetics of Histone Deacetylases. Nature Chemical Biology 2010;6:238-43.

40. Novotny-Diermayr V, Sangthongpitag K, Hu CY, Wu X, Sausgruber N, Yeo P, et al. SB939, a novel potent and orally active histone deacetylase inhibitor with high tumor exposure and efficacy in mouse models of colorectal cancer. Molecular Cancer Therapeutics 2010;9:642-52.

41. Clocchiatti A, Di Giorgio E, Demarchi F, Brancolini C. Beside the MEF2 axis: unconventional functions of HDAC4. Cell Signal 2013;25:269-76.

42. Laubach JP, Moreau P, San-Miguel JF, Richardson PG. Panobinostat for the Treatment of Multiple Myeloma. Clinical Cancer Research 2015;21:4767-73.

43. VanderMolen KM, McCulloch W, Pearce CJ, Oberlies NH. Romidepsin (Istodax, NSC 630176, FR901228, FK228, depsipeptide): a natural product recently approved for cutaneous T-cell lymphoma. J Antibiot (Tokyo) 2011;64:525-31.

44. Drappatz J, Lee EQ, Hammond S, Grimm SA, Norden AD, Beroukhim R, et al. Phase I study of panobinostat in combination with bevacizumab for recurrent high-grade glioma. Journal of Neuro-oncology 2012;107:133-8.

45. Bagcchi S. Panobinostat active against diffuse intrinsic pontine glioma. Lancet Oncology 2015;16:e267.

Figure legends

Fig. 1. PME-1 depletion induces glioma cell synthetic lethality in combination with kinase inhibitor therapies. (**A**) Human glioblastoma T98G cells transfected with Scrambled (Scr.) (grey bars) or PME-1 (black bars) siRNA (for 48 hours) were treated with indicated concentration of different kinase inhibitor compounds. Each bar represents the mean (+ S.E.) percentage of nuclei in sub-G_0/G_1 phase. *p<0.05 and **p<0.001 by Student's t-test. PME-1 siRNA and STS-mediated synthetic lethality assessment by colony growth assay in (**B**) T98G and (**C**) U251MG cells. (**D**) PME-1 siRNA and STS-mediated synthetic lethality between normal astrocytes isolated from rat hippocampus and human glioblastoma T98G cells. PME1-HR siRNA targets both human and rat PME-1 (Supplementary Fig. S1G). Mean + S.E. (**E**) Caspase -3 and -7 activity. Each bar represents mean + S.E. luminescence (relative light unit – RLU) values produced by the cleavage of caspase-3/7 substrate. *p<0.05 by Student's t-test. (**F**) siRNA transfected T98G cells were pre-treated with pan-caspase inhibitor, Z-VAD-FMK for 24 hours followed by STS treatment (24 hours) and analyzed by nuclear fragmentation assay. Mean + S.E. (**G**) Nuclear fragmentation analysis in siRNA transfected T98G cells and treated with STS. Mean + S.E. **p<0.001 by Student's t-test. (**H**) Nuclear fragmentation analysis in T98G cells treated with Bcl-2/xL inhibitor ABT263 with or without STS treatment.

Fig. 2. PME-1 depletion sensitizes glioma cell lines and glioma stem cells (GSCs) to clinically relevant indolocarbazoles. (**A**) Apoptosis analysis in PME-1 depleted

T98G cells with indolocarbazole derivatives. Values are mean + S.E.. *p<0.05 and **p<0.001 by Student's t-test. Representative colony formation assay images and quantifications for siRNA transfected (**B**) T98G and (**C**) U251MG cells with STS derivatives (48 hours). Mean + S.E. *p<0.05 and **p<0.001 by Student's t-test. (**D**) Quantification of bioluminescence (flux - photons/second) signal from Scr. (siScr) or PME-1 (siPME-1) silenced U87MG-luc tumor cells in mice treated with UCN-01 (n=6). Arrows indicate days when mice received UCN-01 treatment. Values are fold change mean flux relative to day-5 (starting day of UCN-01 treatment) +/- S.E. *p<0.05 by Student's t-test. (**E**) Images of tumors isolate from mice (# 1 - 6) on the final day of the experiment (day-16). Representative images and quantitation of colony formation assay in GSC lines (**F**) E2 and (**G**) R10 after PME-1 silencing (48 hours) combined with STS or UCN-01 treatment (48 hours). Mean + S.E. *p<0.05 and **p<0.001 by Student's t-test.

Fig. 3. Reactivation of PME-1 dependent PP2A complexes is required for synthetic lethality with kinase inhibitors. (**A**) Phosphatase activity of PP2A immunoprecipitates (IP) isolated from siRNA transfected T98G cells. Immunoblot shows PP2A C-subunit (PP2Ac) levels in IP. Mean + S.E. *p<0.05. (**B**) Okadaic acid (OA) blocks the PME-1 siRNA-mediated synthetic lethality. Mean + S.E. fold change of 50 nM STS treated samples over respective untreated samples. (**C**) Cartoon picture of the PP2A trimeric complex depicting also cellular PP2A-inhibitory proteins (red lines) and chemical PP2A inhibitors and activators (black lines). Comparison of apoptosis induction in (**D**) CIP2A or PME-1 silenced or (**E**) PP2A activator (FTY720, Selenate,

Xylulose-5-phosphate – X5P) treated cells with STS. Mean + S.E. *p<0.05, NS – no significant difference. (**F**) Apoptosis in T98G cells co-depleted for PME-1 and indicated PP2A B-subunit with 50nM STS. Mean + S.E. *p<0.05, **p<0.001 by Student's t-test. (**G**) Genetic alterations in PP2A subunits in TCGA GBM data by cBioPortal program (n=281).

Fig. 4. HDAC4 is involved in glioma cell kinase inhibitor resistance. T98G cells (**A**) treated with specific chemical inhibitors or (**B**) transfected with siRNA for indicated PP2A target proteins were analyzed for apoptosis induction upon STS treatment. Values are mean + S.E. (**C**) Total protein lysates from (A) subjected to immunoblotting with indicated antibodies. (**D**) Colony growth assay of siRNA transfected T98G cells and treated with 30 nM STS (48 hours) (**E**) WB analysis of T98G cells as in (D). (**F**) Correlation between sensitivity of PME-1 and HDAC4 depleted cells towards STS derivatives. Pearson's correlation coefficient R between +0.4 to + 0.69 corresponds to strong positive relationship. (**G**) Colony growth assay of HDAC4 silenced T98G cells treated with STS analogues. Colony growth assay in (**H**) E2 and (**I**) R10 glioma stem cell lines upon HDAC4 silencing and treatment with STS or UCN-01. Bottom graphs display quantification of colony growth. Mean + S.E. *p<0.05 and **p<0.001 by Student's t-test. (**J**) Apoptosis in T98G cells silenced for PME-1 and HDAC4 alone or in combination (48 hours) and treated with STS (30nM or 50 nM for 24 hours). Mean + S.E. NS – no significant difference by Student's t-test. (**K**) siRNA transfected T98G cells treated with STS were analyzed by nuclear fragmentation assay. Mean + S.E. (**L**) Apoptosis induction in T98G cells silenced for HDAC4 and PPP2R2A B-subunit were

treated with STS (50 nM). Mean + S.E. (**M**) Proximity ligation assay (PLA) in T98G cells using HDAC4 and PP2A C-subunit (PP2A-Cα) or PPP2R2A B-subunit antibodies. Green dots: HDAC4-PP2A-Cα interaction; Red dots HDAC4-PPP2R2A interaction. Nuclei stained by DAPI (blue). Negative control staining was performed at similar conditions excluding the primary antibodies.

Fig. 5. PME-1 regulates cytosolic HDAC4. (**A**) Immunofluorescence for HDAC4 (green) showing mainly cytosolic localization in T98G cells (40X magnification). (**B**) Immunohistochemical (IHC) staining of cytosolic HDAC4 in human astrocytic glioma (grade III and IV) tumor samples. Insets from the representative images shown in Fig. 6A. (**C**) T98G cells transfected with HDAC4-GFP and Scr. or PME-1 siRNA were analysed by fluorescence microscopy. Bars represent the percentage of cells showing cytoplasmic (green bars) or nuclear (blue bars) HDAC4-GFP expression. Mean + S.E. *$p<0.05$ by Student's t-test. (**D**) Cytosolic lysates from T98G cells transfected with Scr, PME-1 or HDAC4 siRNA (72 hours) immunoblotted with pan-acetylated lysine (ac-lysine) antibody. Arrows indicate specific bands similarly up-regulated in PME-1 or HDAC4 silenced cells. (**E**) Phospho-Ser 632 HDAC4 and total HDAC4 immunoblotting from whole cell lysates of T98G cells transfected with indicated siRNA, and treated with STS (50 nM) for 6 hours. Quantification of HDAC4 expression normalized to GAPDH shown in the bottom graph. Mean + S.E. *$p<0.05$ and **$p<0.001$ by Student's t-test. (**F**) HDAC4 inhibitory profile of the HDAC inhibitors, FK228, Panobinostat and SAHA. The inhibitory constant Ki values [μM] are as reported in previous studies. Cell viability WST-1 assay in T98G cells treated with increasing concentration of (**G**) FK228 or (**H**)

Panobinostat either alone or in combination with STS or UCN-01. Mean +/- S.E. (**I**) Apoptosis analysis in T98G cells treated with Panobinostat or SAHA either alone or in combination with STS or UCN-01. Mean + S.E.

Fig. 6. Therapeutic vulnerability in human gliomas based on PME-1/HDAC4/BAD status. (**A**) Representative images of PME-1, HDAC4 and BAD IHC-staining (scored 0 to 3) from human astrocytic glioma patient samples (n=139 for HDAC4, n=119 for BAD). Percentage of the patient samples with respective staining intensity score are indicated at the bottom right corner of each image. (**B**) Correlation between HDAC4 expression and astrocytic glioma tumor grade. p=0.000 by Pearson Chi-square test. (**C**) T98G shRNA clones with control shRNA (GFP#1 and #2) or PME-1 shRNA (PME#1 and #2) were lysed and blotted with PME-1 antibody. (**D**) Representative images of T98G shRNA clones treated with STS derivatives, K252a or CEP-701 for 48 hours and subjected to colony growth assay. (**E**) Quantifications (mean + S.E.) of colony growth assay as in (B). *p<0.05 by Student's t-test. BAD immunostaining correlation with (**F**) PME-1 or (**G**) HDAC4 immunostaining. Red boxes depict the patient subgroup with PME-1^{low}/BAD^{high} or $HDAC4^{low}$/BAD^{high} phenotypes, and blue box with $HDAC4^{high}$/BAD^{high} phenotype. The percentage of patients with stratification phenotypes is indicated at the bottom of the table. (**H**) Schematic representation of the glioma patient stratification strategy based on patient tumor IHC analysis for PME-1, HDAC4 and BAD expression for proposed therapy with multikinase inhibitor (MKI) alone or in combination with HDAC4 inhibitors.

Figure 1

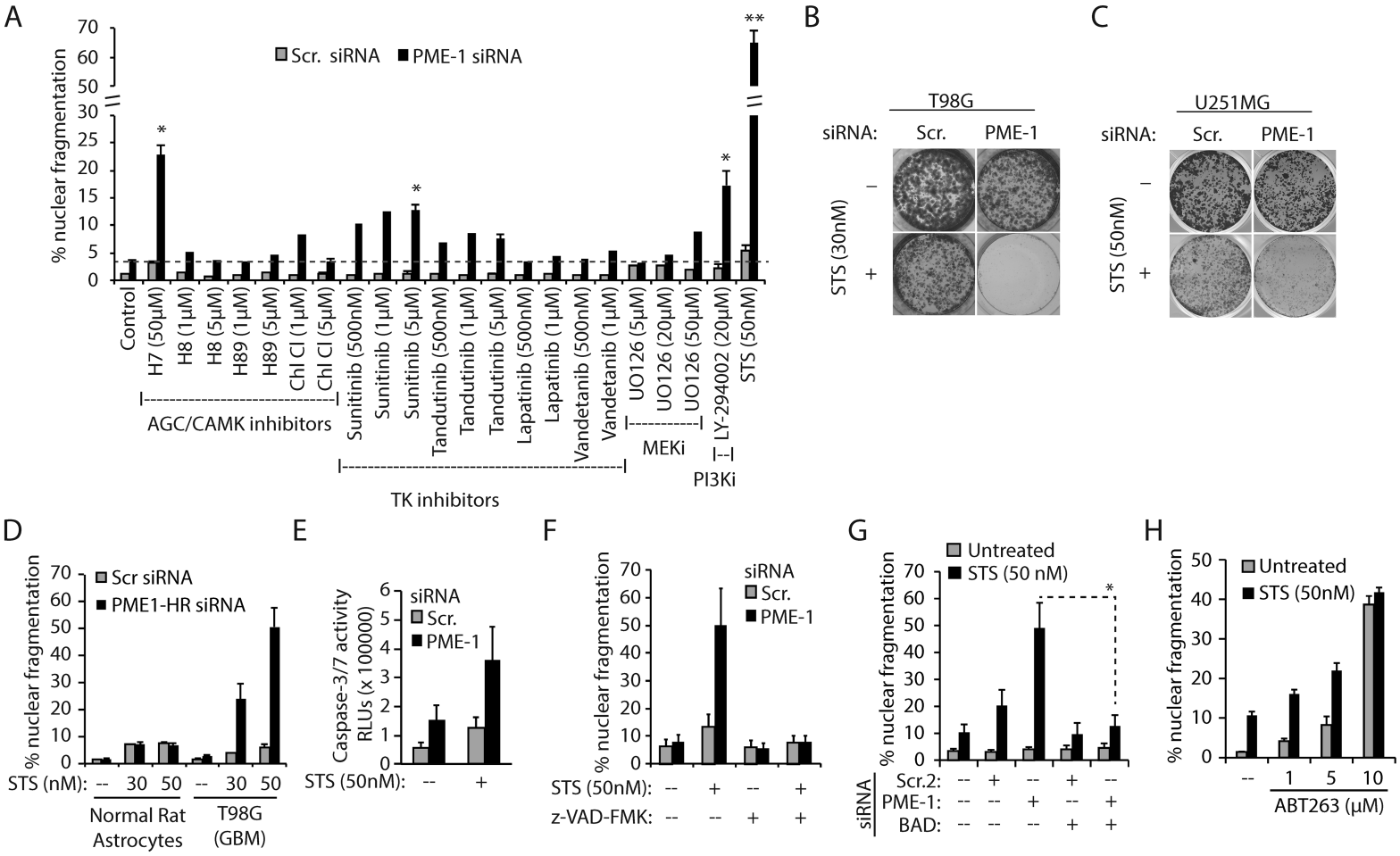
A
% nuclear fragmentation
Scr. siRNA
PME-1 siRNA
Control
H7 (50μM)
H8 (1μM)
H8 (5μM)
H89 (1μM)
H89 (5μM)
ChI CI (1μM)
ChI CI (5μM)
Sunitinib (500nM)
Sunitinib (1μM)
Sunitinib (5μM)
Tandutinib (500nM)
Tandutinib (1μM)
Tandutinib (5μM)
Lapatinib (500nM)
Lapatinib (1μM)
Vandetanib (500nM)
Vandetanib (1μM)
UO126 (5μM)
UO126 (20μM)
UO126 (50μM)
LY-294002 (20μM)
STS (50nM)
AGC/CAMK inhibitors
TK inhibitors
MEKi
PI3Ki
B
T98G
siRNA:
Scr.
PME-1
STS (30nM)
C
U251MG
siRNA:
Scr.
PME-1
STS (50nM)
D
% nuclear fragmentation
Scr siRNA
PME1-HR siRNA
STS (nM):
Normal Rat Astrocytes
T98G (GBM)
E
Caspase-3/7 activity RLUs (x 100000)
siRNA
Scr.
PME-1
STS (50nM):
F
% nuclear fragmentation
siRNA
Scr.
PME-1
STS (50nM):
z-VAD-FMK:
G
% nuclear fragmentation
Untreated
STS (50 nM)
siRNA
Scr.2:
PME-1:
BAD:
H
% nuclear fragmentation
Untreated
STS (50nM)
ABT263 (μM)

Figure 2

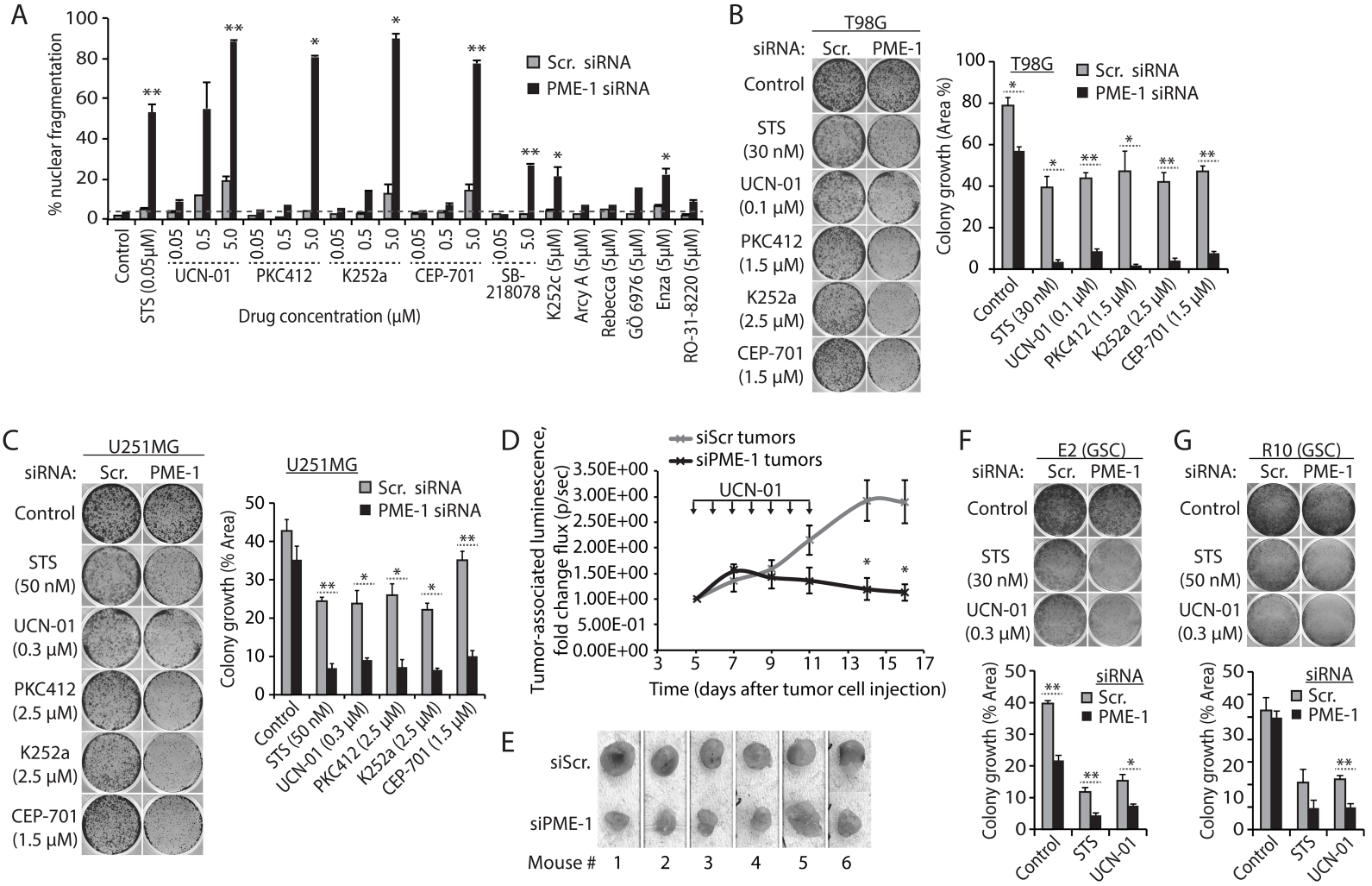
A
% nuclear fragmentation
Scr. siRNA
PME-1 siRNA
Control
STS (0.05μM)
UCN-01
PKC412
K252a
CEP-701
SB-218078
K252c (5μM)
Arcy A (5μM)
Rebecca (5μM)
GÖ 6976 (5μM)
Enza (5μM)
RO-31-8220 (5μM)
Drug concentration (μM)
B
T98G
siRNA: Scr. PME-1
Control
STS (30 nM)
UCN-01 (0.1 μM)
PKC412 (1.5 μM)
K252a (2.5 μM)
CEP-701 (1.5 μM)
Colony growth (Area %)
C
U251MG
D
siScr tumors
siPME-1 tumors
UCN-01
Tumor-associated luminescence, fold change flux (p/sec)
Time (days after tumor cell injection)
E
siScr.
siPME-1
Mouse # 1 2 3 4 5 6
F
E2 (GSC)
siRNA
G
R10 (GSC)

Figure 3

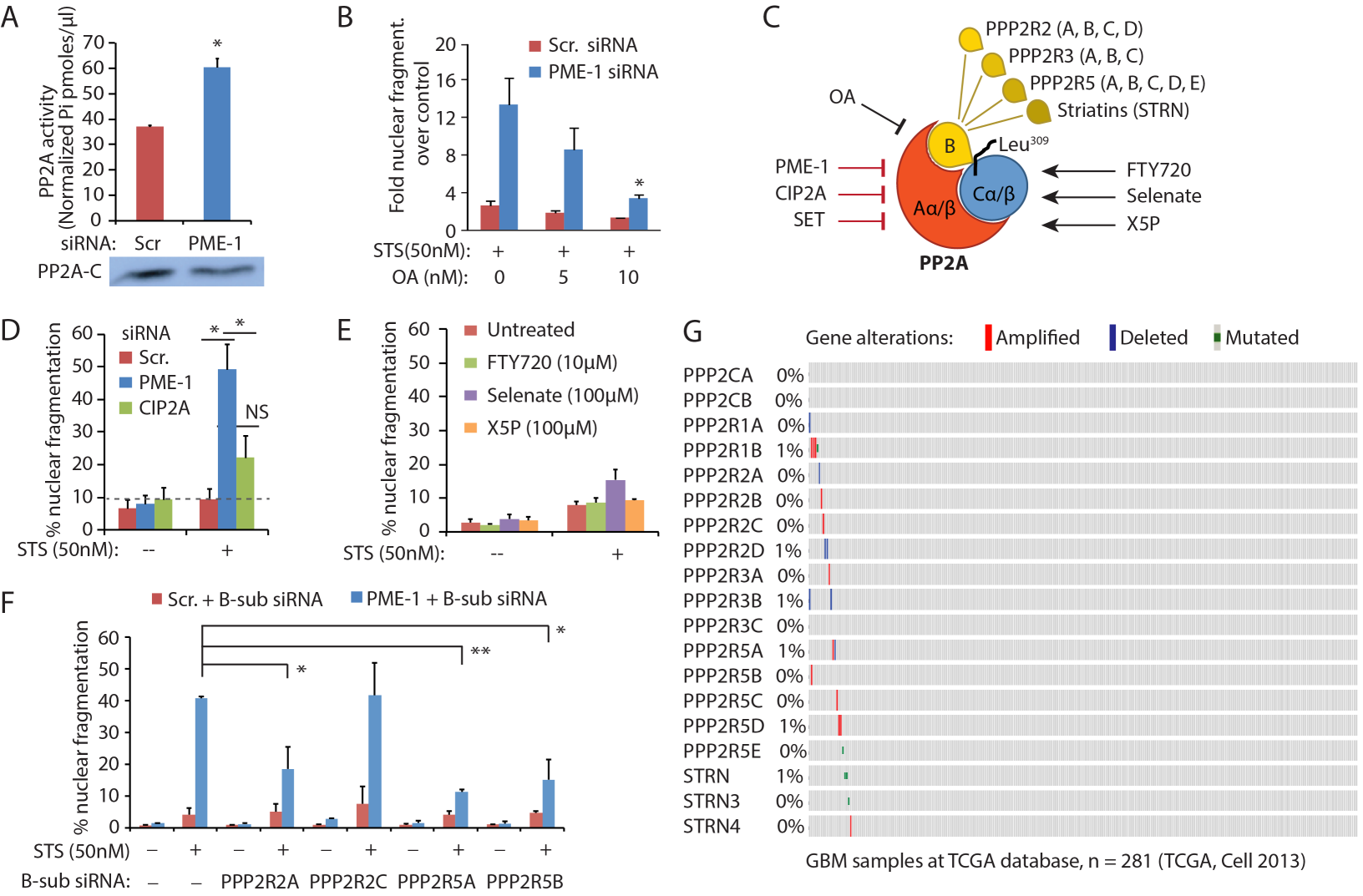
A
PP2A activity (Normalized Pi pmoles/µl)
siRNA: Scr PME-1
PP2A-C
B
Fold nuclear fragment. over control
Scr. siRNA
PME-1 siRNA
STS(50nM): + + +
OA (nM): 0 5 10
C
PPP2R2 (A, B, C, D)
PPP2R3 (A, B, C)
PPP2R5 (A, B, C, D, E)
Striatins (STRN)
OA
B
Leu309
PME-1
CIP2A
SET
Aα/β
Cα/β
FTY720
Selenate
X5P
PP2A
D
% nuclear fragmentation
siRNA
Scr.
PME-1
CIP2A
NS
STS (50nM): -- +
E
% nuclear fragmentation
Untreated
FTY720 (10µM)
Selenate (100µM)
X5P (100µM)
STS (50nM): -- +
F
Scr. + B-sub siRNA
PME-1 + B-sub siRNA
% nuclear fragmentation
STS (50nM) – + – + – + – + – +
B-sub siRNA: – – PPP2R2A PPP2R2C PPP2R5A PPP2R5B
G
Gene alterations: Amplified Deleted Mutated
PPP2CA 0%
PPP2CB 0%
PPP2R1A 0%
PPP2R1B 1%
PPP2R2A 0%
PPP2R2B 0%
PPP2R2C 0%
PPP2R2D 1%
PPP2R3A 0%
PPP2R3B 1%
PPP2R3C 0%
PPP2R5A 1%
PPP2R5B 0%
PPP2R5C 0%
PPP2R5D 1%
PPP2R5E 0%
STRN 1%
STRN3 0%
STRN4 0%
GBM samples at TCGA database, n = 281 (TCGA, Cell 2013)

Figure 4

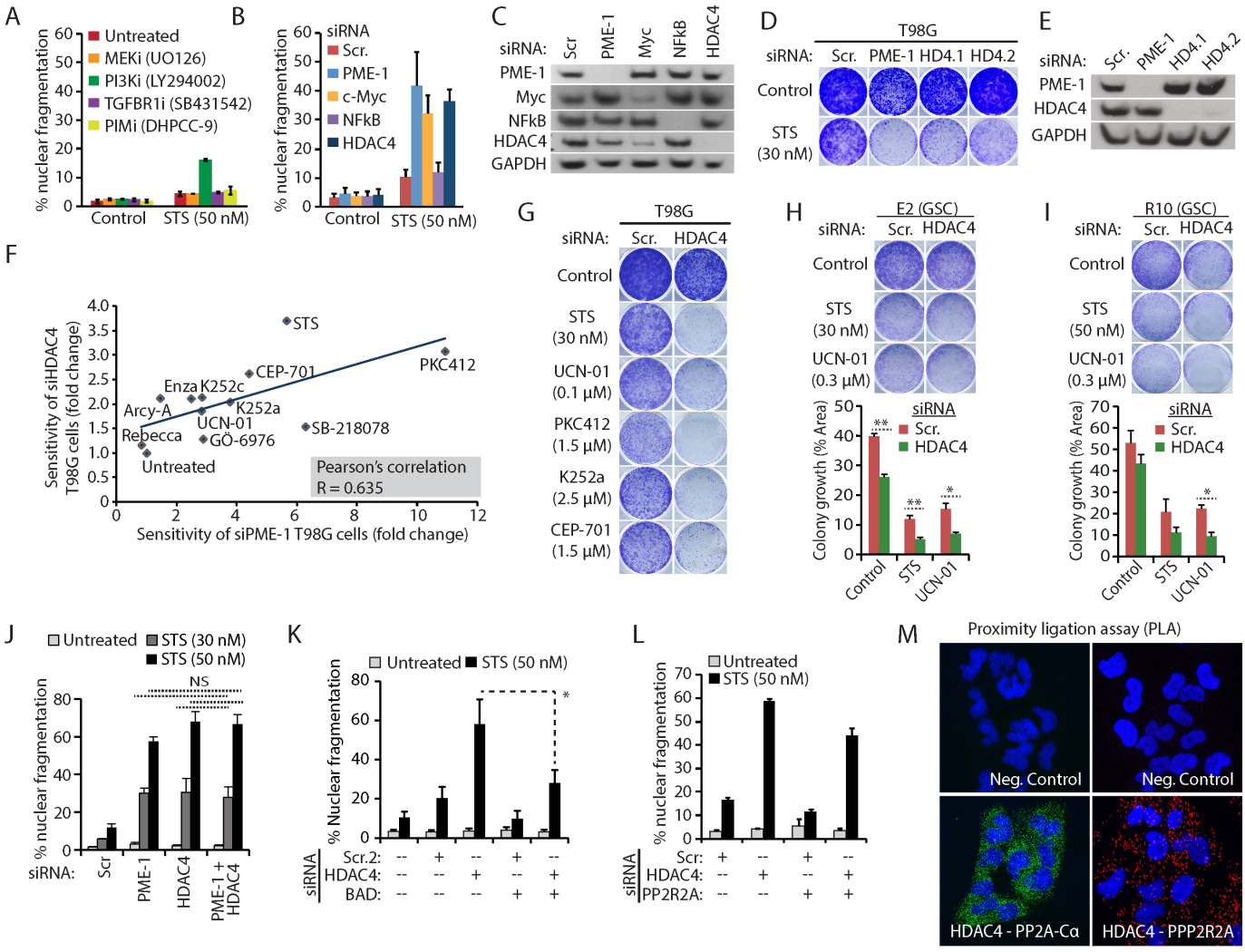
A
% nuclear fragmentation
Untreated
MEKi (UO126)
PI3Ki (LY294002)
TGFBR1i (SB431542)
PIMi (DHPCC-9)
Control
STS (50 nM)
B
siRNA
Scr.
PME-1
c-Myc
NFkB
HDAC4
C
siRNA:
PME-1
Myc
NFkB
HDAC4
GAPDH
D
T98G
Control
STS (30 nM)
E
HDAC4
F
Sensitivity of siHDAC4 T98G cells (fold change)
Sensitivity of siPME-1 T98G cells (fold change)
STS
CEP-701
PKC412
Enza
K252c
Arcy-A
K252a
UCN-01
Rebecca
GÖ-6976
SB-218078
Untreated
Pearson's correlation
R = 0.635
G
T98G
Control
STS (30 nM)
UCN-01 (0.1 μM)
PKC412 (1.5 μM)
K252a (2.5 μM)
CEP-701 (1.5 μM)
H
E2 (GSC)
UCN-01 (0.3 μM)
Colony growth (% Area)
I
R10 (GSC)
STS (50 nM)
J
Untreated
STS (30 nM)
STS (50 nM)
NS
K
L
M
Proximity ligation assay (PLA)
Neg. Control
HDAC4 - PP2A-Cα
HDAC4 - PPP2R2A

Figure 5

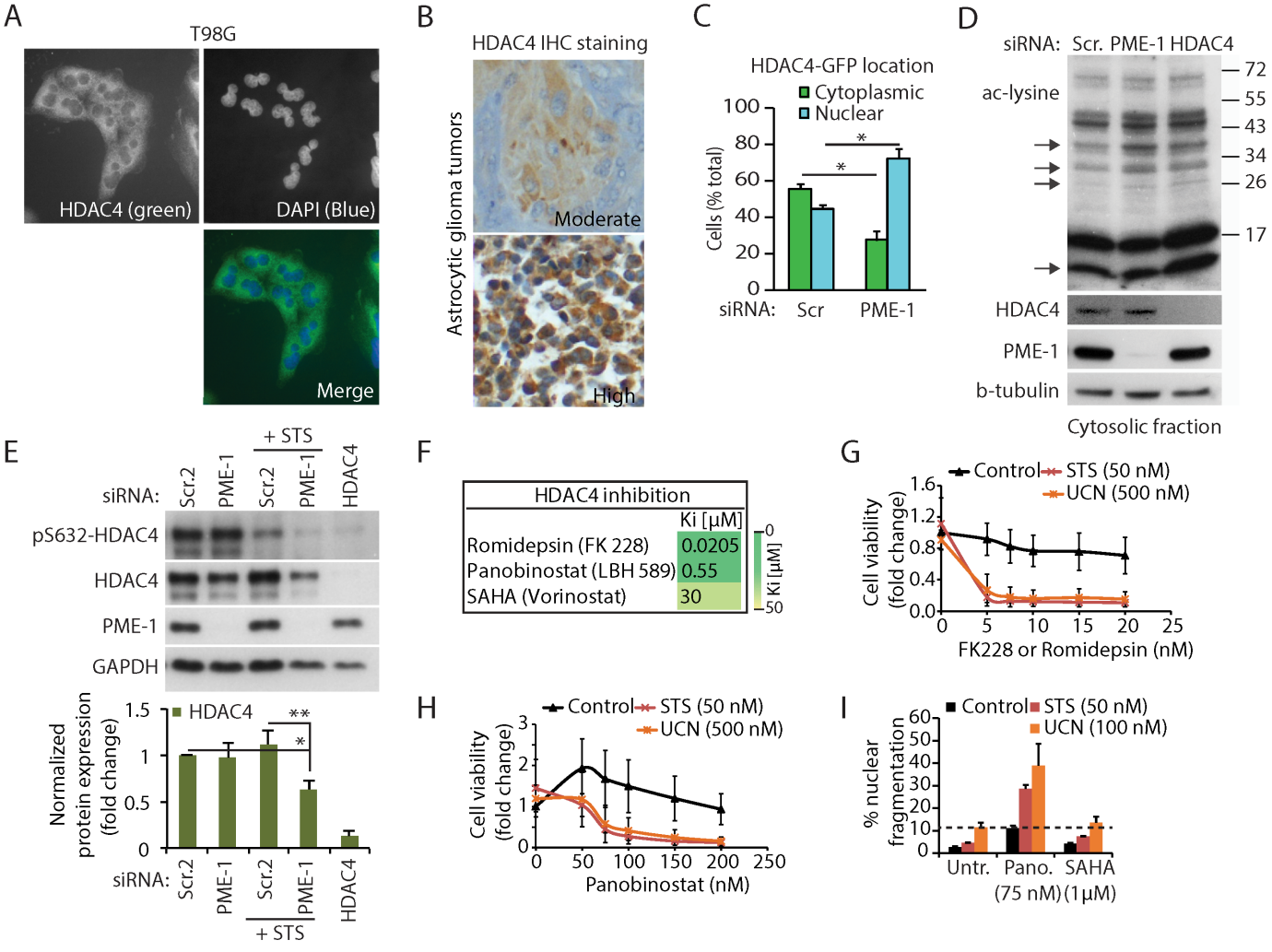
A
T98G
HDAC4 (green)
DAPI (Blue)
Merge
B
HDAC4 IHC staining
Astrocytic glioma tumors
Moderate
High
C
HDAC4-GFP location
Cytoplasmic
Nuclear
Cells (% total)
siRNA: Scr PME-1
D
siRNA: Scr. PME-1 HDAC4
ac-lysine
HDAC4
PME-1
b-tubulin
Cytosolic fraction
E
+ STS
siRNA: Scr.2 PME-1 Scr.2 PME-1 HDAC4
pS632-HDAC4
HDAC4
PME-1
GAPDH
Normalized protein expression (fold change)
F
HDAC4 inhibition
Ki [μM]
Romidepsin (FK 228) 0.0205
Panobinostat (LBH 589) 0.55
SAHA (Vorinostat) 30
G
Control
STS (50 nM)
UCN (500 nM)
Cell viability (fold change)
FK228 or Romidepsin (nM)
H
Panobinostat (nM)
I
UCN (100 nM)
% nuclear fragmentation
Untr.
Pano. (75 nM)
SAHA (1μM)

Figure 6

A

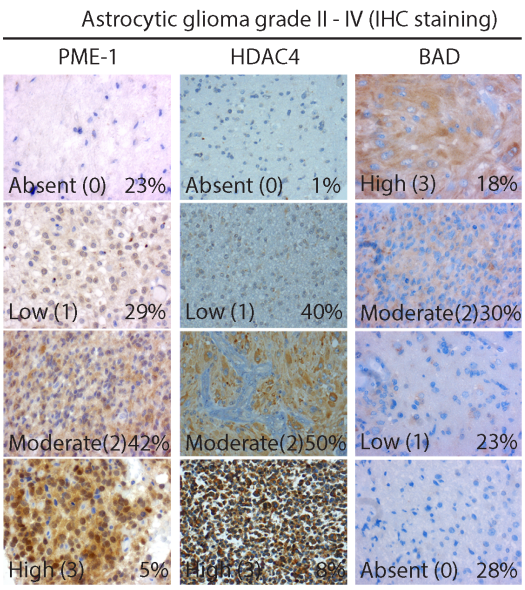

Magnification x400

B

HDAC4 staining	Astrocytic glioma tumor grade II	III	IV	Total
	12	25	102	n=139
Absent (0)	2 (100 %)	0 (0 %)	0 (0 %)	2
Low (1)	6 (11 %)	8 (14 %)	42 (75 %)	56
Moderate (2)	4 (6 %)	14 (20 %)	52 (74 %)	70
High (3)	0 (0 %)	3 (27 %)	8 (73 %)	11

Pearson chi-square test p=0.000

C

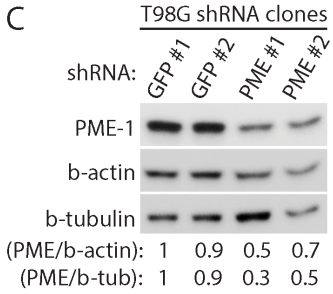

D

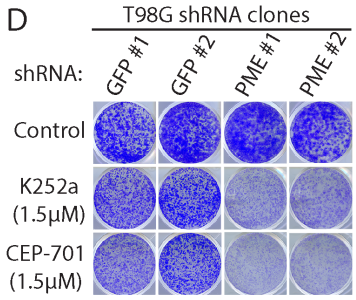

E

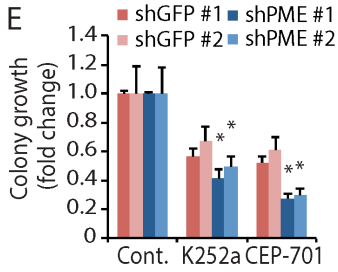

F

BAD staining	PME-1 staining (Cytosolic) (0)	(1)	(2)	(3)	Total
	26	31	45	7	n=109
Absent (0)	15	7	8	1	31
Low (1)	7	9	6	2	24
Moderate (2)	3	12	15	3	33
High (3)	1	3	16	1	21

PME-1^{low} BAD^{high} = 17.4 % (19 of 109)

G

BAD staining	HDAC4 staining (0)	(1)	(2)	(3)	Total
	2	51	57	9	n=119
Absent (0)	2	19	12	1	34
Low (1)	0	18	9	0	27
Moderate (2)	0	10	22	4	36
High (3)	0	4	14	4	22

HDAC4^{low} BAD^{high} = 11.7 % (14 of 119)

HDAC4^{high} BAD^{high} = 37.0 % (44 of 119)

H